EUROPHYSICS LETTERS 15 November 2005

Europhys. Lett., **72** (4), pp. 671–677 (2005)
DOI: 10.1209/epl/i2005-10279-7

Shape-induced capillary interactions of colloidal particles

E. A. van Nierop[1,2], M. A. Stijnman[2] and S. Hilgenfeldt[3,4,2]

[1] *Division of Engineering and Applied Sciences, Harvard University Cambridge, MA 02138, USA*
[2] *University of Twente, Faculty of Applied Physics, Physics of Fluids P.O. Box 217, 7500 AE Enschede, the Netherlands*
[3] *Department of Engineering Sciences and Applied Mathematics Northwestern University - Evanston, IL 60208, USA*
[4] *Department of Mechanical Engineering, Northwestern University Evanston, IL 60208, USA*

received 27 July 2005; accepted 21 September 2005
published online 14 October 2005

PACS. 82.70.Dd – Colloids.
PACS. 68.03.Cd – Surface tension and related phenomena.

Abstract. – We show that near-spherical micrometer-sized colloidal particles at an interface of two fluids experience inter-particle forces merely as a consequence of their shape-induced capillary interaction. The interaction is strong even if the deviations from sphericity are on the nm-scale, and can hardly be avoided in experiment. For particles of 2 μm radius, a deformation of 20 nm can result in an attractive potential of $2k_BT$ at a distance of 4 particle radii. Dynamical simulations of many particles confirm that the forces lead to aggregates of dendritic or hexagonal-lattice type. The latter pattern exhibits strong herringbone-phase orientational order.

Introduction. – Colloidal particles trapped at the interface between two fluids (air/water, oil/water, etc.) form various patterns, from 2D crystals to foam-like polygonal patterns and fractal-like aggregates [1–5]. To explain such patterns, knowledge of the much debated interaction potential between particles is required. Apart from van der Waals attraction and electrostatic dipole-dipole repulsion (for charged particles) a number of extra contributions have been suggested. Chan *et al.* [6] consider the deformation of the interface by the weight of the particles; this potential contribution is negligible (*i.e.*, much smaller than k_BT) for (polystyrene) particles smaller than 10 μm diameter. Stamou *et al.* [7] consider the effect of a (very) rough contact line and calculate that the associated potential can be as much as $10^4 k_BT$ for particles of 1 μm diameter. A Casimir-like attraction from thermal fluctuations of the interface has also been discussed [8, 9].

In this paper, we show that even uncharged colloidal particles, in the absence of gravitational effects or contact line roughness, will experience mutual attraction or repulsion if they are slightly *non-spherical*. The particle shape induces an undulating contact line and a substantial inter-particle potential contribution analogous to that in [7]. In contrast to previous studies, we quantify the contact line deformation directly from the particle shape. In addition, we explicitly demonstrate and calculate pattern formation. In experiment, the shape-induced potential contribution should always be present as no particle is ever perfectly spherical. For

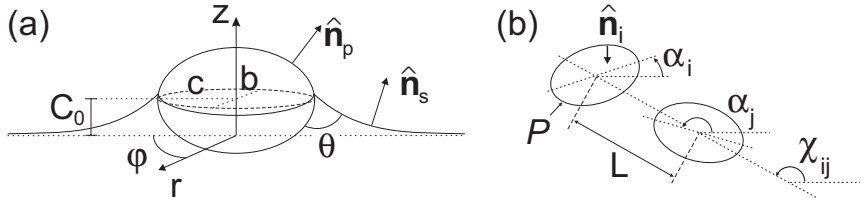

Fig. 1 – (a) Particle and interface geometry parameters. (b) Sketch of the coordinate system and geometry for multiple particle simulations.

example, our calculations show a significant attraction ($2k_BT$) at a separation of 4 particle radii for particles of 2 μm radius with only a 1% deformation (*i.e.* 20 nm) from sphericity.

Contact line determination. – Figure 1a shows a spheroidal particle with semi-axes c and b ($c > b$) at an interface between two fluids. We use the spheroid as a representation of a slightly deformed sphere. Other deformations can be treated analogously using a shape expansion, *e.g.* into spherical harmonics. We exclude gravitational surface deformation, which produces attractive potentials $\ll k_BT$ for particles of around 1 micron radius (alternatively, we can think of the particle and the fluids as density-matched). Interfaces with small deformations from flatness are described by a function $z(r, \varphi)$ in polar coordinates. Since only surface energy is present, the equilibrium interface is a minimal surface [10] which fulfills

$$\nabla^2 z + \frac{2}{r^3} z_\varphi^2 z_r + \frac{1}{r^2} z_{\varphi\varphi} z_r^2 + \frac{1}{r} z_r^3 - \frac{2}{r^2} z_\varphi z_r z_{r\varphi} + \frac{1}{r^2} z_\varphi^2 z_{rr} = 0\,. \tag{1}$$

The components of the Laplacian dominate the other terms by $\mathcal{O}(z^2/r^2)$. The multipole solution to Laplace's equation, taking into account the fore-aft symmetry of the ellipsoid, is

$$z_s(r, \varphi) = \sum_{n=1}^{\infty} \frac{C_{2n}}{r^{2n}} \cos(2n\varphi), \tag{2}$$

where the subscript s denotes the fluid/fluid interface. This reduces the problem to finding the coefficients C_{2n}. Two boundary conditions are imposed at the contact line described by $[\varphi, z_c(\varphi), r_c(\varphi)]$:

$$z_s = z_p \;=\; z_c(\varphi) \text{ at } r = r_c(\varphi), \tag{3}$$

$$\hat{\boldsymbol{n}}_s \cdot \hat{\boldsymbol{n}}_p \;=\; \cos(\theta) \text{ at } r = r_c(\varphi). \tag{4}$$

The first ensures continuity of the interface at the contact line (z_p designates a point on the spheroidal particle), the second enforces the thermodynamic contact angle θ at every position φ, as $\hat{\boldsymbol{n}}_s$ and $\hat{\boldsymbol{n}}_p$ are unit normal vectors to the fluid interface and the particle, respectively. Points on the spheroid (fig. 1a) are described by

$$(\tilde{z}_p - C_0)^2 = 1 - \tilde{r}^2(1 - e^2 \cos^2 \varphi), \tag{5}$$

where $e = \sqrt{1 - \frac{b^2}{c^2}}$ is the eccentricity of the particle and $\tilde{z}_p = z_p/b, \tilde{r} = r/b$ (from now on we will drop the tilde). For a perfect sphere ($e = 0$), (4) is fulfilled by a flat interface and circular contact line ($\hat{\boldsymbol{n}}_s = \hat{\boldsymbol{e}}_z$), so that $C_0 = -\cos(\theta)$ and $C_{2n} = 0$ for all $n \geq 1$. However, for finite e, r_c and z_c are functions of φ and the contact line undulates. The multipole coefficients can then be determined numerically, or approximated analytically.

TABLE I – *Coefficients C_{2n} for several eccentricities and contact angles. These values of e correspond to $c/b = 1.001, 1.01,$ and 1.1. The right-most column shows the relative deviation $\delta C_2 = (K_2 e^2 - C_2)/C_2$ of the analytical approximation from the numerical contact line integration.*

θ	e	C_0	C_2	C_4	C_6	C_8	δC_2
100	0.045	0.174	$2.72 \cdot 10^{-5}$	$2.86 \cdot 10^{-8}$	$2.69 \cdot 10^{-10}$	$1.33 \cdot 10^{-10}$	$2.20 \cdot 10^{-3}$
	0.14	0.173	$2.74 \cdot 10^{-4}$	$2.88 \cdot 10^{-6}$	$3.71 \cdot 10^{-8}$	$3.21 \cdot 10^{-10}$	$2.19 \cdot 10^{-2}$
	0.42	0.166	$2.92 \cdot 10^{-3}$	$3.21 \cdot 10^{-4}$	$4.34 \cdot 10^{-5}$	$6.49 \cdot 10^{-6}$	$1.91 \cdot 10^{-1}$
120	0.045	0.500	$4.69 \cdot 10^{-5}$	$3.90 \cdot 10^{-8}$	$1.77 \cdot 10^{-10}$	$-2.99 \cdot 10^{-12}$	$2.60 \cdot 10^{-3}$
	0.14	0.498	$4.74 \cdot 10^{-4}$	$3.96 \cdot 10^{-6}$	$4.10 \cdot 10^{-8}$	$6.02 \cdot 10^{-10}$	$2.58 \cdot 10^{-2}$
	0.42	0.483	$5.21 \cdot 10^{-3}$	$4.65 \cdot 10^{-4}$	$5.11 \cdot 10^{-5}$	$6.24 \cdot 10^{-6}$	$2.20 \cdot 10^{-1}$
140	0.045	0.766	$2.18 \cdot 10^{-5}$	$1.04 \cdot 10^{-8}$	$3.57 \cdot 10^{-12}$	$6.68 \cdot 10^{-13}$	$3.20 \cdot 10^{-3}$
	0.14	0.764	$2.22 \cdot 10^{-4}$	$1.06 \cdot 10^{-6}$	$6.35 \cdot 10^{-9}$	$2.28 \cdot 10^{-11}$	$3.17 \cdot 10^{-2}$
	0.42	0.751	$2.57 \cdot 10^{-3}$	$1.35 \cdot 10^{-4}$	$8.83 \cdot 10^{-6}$	$6.47 \cdot 10^{-7}$	$2.63 \cdot 10^{-1}$

Numerical calculation of coefficients. – Using (5) to replace r^2 in (2), and then using (3) yields an implicit equation for $z_c(\varphi)$,

$$\sum_{n=1}^{\infty} \frac{C_{2n}}{(1-(z_c-C_0)^2)^n} \cos(2n\varphi)(1-e^2\cos^2\varphi)^n - z_c = 0. \tag{6}$$

We truncate (6) at $n \leq 50$ and use a Newton-Raphson algorithm with an initial set of C_{2n} to obtain an approximation of z_c for a set of φ. With (5), r_c values follow, and $\hat{\boldsymbol{n}}_s$ and $\hat{\boldsymbol{n}}_p$ can be computed at the contact line. The set of coefficients C_{2n} must now be optimized in order to fulfill (4). We discretize $G \equiv \int_\Gamma \left(\hat{\boldsymbol{n}}_s \cdot \hat{\boldsymbol{n}}_p - \cos(\theta)\right)^2 \mathrm{d}s$, using 90 equidistant values of φ on the line Γ which, for symmetry reasons, is taken as one quarter of the full contact line. The multidimensional minimization of G with respect to the C_{2n} was done with the simplex method [11]. Table I lists the first few coefficients for different values of e and θ.

Analytical calculation of coefficients. – It is desirable to have an analytical result for C_{2n} as well, to speed up calculations and clarify the scaling of the interaction with the system parameters. We expand the contact line *simultaneously* in even multipole components and powers of squared eccentricity (e^2). We write the multipole components as powers of $\mu^2 \equiv \cos^2\varphi$, using $\cos(2n\varphi) = T_{2n}(\mu)$, where T_{2n} are the even Chebyshev polynomials. With this nomenclature, the spheroidal particle surface (5) is described by $z_p = C_0 - \left(1 - r^2(1-e^2\mu^2)\right)^{1/2}$, from which $\hat{\boldsymbol{n}}_p$ is obtained. We further use the assumption (later shown to be self-consistent) that every multipole order $2n$ can be satisfied by terms of order e^{2n}, *i.e.* we rewrite $C_{2n} = K_{2n}e^{2n}$ in (2), where $K_{2n} = \mathcal{O}(1)$ for all n. To determine $r_c(\varphi)$, we apply the expansion

$$r_c = r_{00} + r_{02}e^2 + r_{20}\mu^2 + r_{22}e^2\mu^2 + \ldots \tag{7}$$

to (3) and (4) and equate equal orders of e^2 and μ^2. Truncating at $n = 1$ uniquely determines $r_{00} = \sin\theta$, $r_{20} = 0$, $r_{02} = -\sin\theta(1+\cos^2\theta)/6$, $r_{22} = \sin\theta(3+\cos^2\theta)/6$, as well as $C_0 = -\cos\theta + e^2\cos\theta(2+\sin^2\theta)/4$ and $K_2 = -\sin^4\theta\cos\theta/12$. The equilibrium position of the particle center (C_0) is thus shifted by $\mathcal{O}(e^2)$, and the interface around the particle, to leading order, is given by

$$z_s = -\frac{e^2}{12r^2}\sin^4\theta\cos\theta\cos 2\varphi\,. \tag{8}$$

Note that (8) peaks at $\theta \approx 63.4°$ and $116.6°$, cf. fig. 2(right). Comparing the coefficients $C_2 = e^2K_2$ to the values obtained numerically (see table I), we find them in excellent agreement for

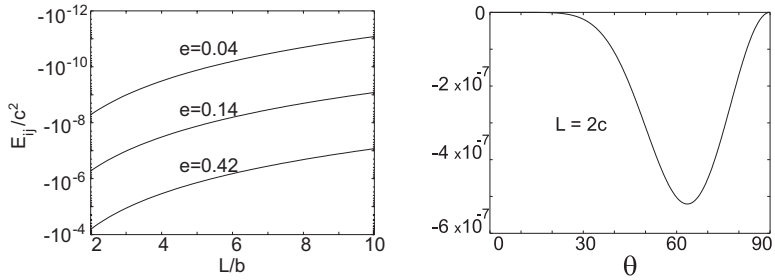

Fig. 2 – Non-dimensionalized potential *vs.* separation for varying (left) eccentricities e and (right) contact angles θ. The potential is stronger for larger particles, smaller separations, and larger deformations. In the left panel $\theta = 120^\circ$ and in the right one $e = 0.14$.

small e, with a relative error of order e^2, as expected. The approximation becomes unreliable for $e \gtrsim 0.2$, so that the more complete numerical algorithms should be employed for simulations of strongly deformed particles (cf. the experiments in [4, 5]).

Particle interaction and aggregate formation. – With surface tension as the only force present in the problem, the interaction potential between particles is given by the gain (or loss) in surface area as their relative position is changed [7]. We use the Nicolson approximation, valid for small e [6, 7, 12, 13], where the interfacial deformation is taken to be the sum of the deformations due to the isolated particles. If a cluster with M particles is already present, the interaction energy between it and one additional free particle i is

$$E_{tot.} = \sum_{j=1}^{M} E_{ij} = 2\sigma \int_P z_i \left(\hat{\boldsymbol{n}}_i \cdot \sum_{j=1}^{M} \nabla z_j \right) \mathrm{d}s_i. \tag{9}$$

Here, σ is the surface tension, z_i, z_j the height of the contact line of particles i, j, and $\hat{\boldsymbol{n}}_i$ is the normal to the *projection* P of the contact line around particle i onto the $z = 0$ plane, pointing away from the area of integration.

Equation (9) contains two assumptions of linearity: i) Nicolson superposition and ii) additivity of particle pair interactions. Both are violated at small interparticle distances, as the equations governing boundary conditions around multiple particles become nonlinear. Once i) is accepted, however, ii) is fulfilled because of the linear dependence of E_{ij} on z_i and ∇z_j (this is unlike the case of membrane interactions [14]). We will focus on the longer-range effects of capillary interaction here, as nonlinear corrections at small particle separations, *e.g.* those discussed in [13, 15], should not alter our qualitative conclusions (see the discussion of numerical results below).

Figure 2 shows $E_{ij}/\sigma c^2$ for two particles, computed with the coefficients of table I. The scaling behaviour expected from (8) is confirmed: since $z_{i,j} \propto e^2$, the curves are separated by a factor $(e_1/e_2)^4$. In absolute terms, E_{ij} is quite large: *e.g.*, at an air/water interface two touching particles with $e = 0.14$ and $c = 2\,\mu$m, experience $E_{ij} \approx 33 k_B T$ at room temperature.

Dynamic simulations of particle aggregation are performed using (9), either by direct computation of the integrals or, for small e, by making use of the analytical results. As the interaction energies typically exceed $k_B T$ considerably, we perform the simulations at zero temperature. Equation (8) describes the deformation induced by a (point) quadrupole, and to this approximation, the interaction energy becomes (cf. [7])

$$E_{ij} = -12 \cos\left[2(\alpha_i + \alpha_j - 2\chi_{ij})\right] \left(\frac{c}{L}\right)^4 \delta E\,, \tag{10}$$

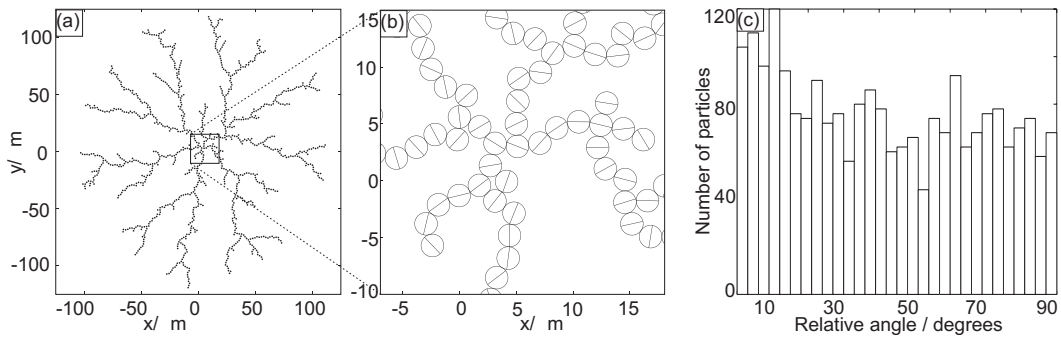

Fig. 3 – (a) Dendritic structure of particles with $e = 0.10$, (b) zoom showing particle alignments, and (c) the corresponding distribution of relative orientations.

where $\delta E = \pi\sigma c^2 C_2^2$. Figure 1b indicates the connector angle χ_{ij} and director angles α_i and α_j used in (10). Using the analytical value for K_2, we have an explicit expression for the interaction energy in terms of particle shape, correct to $\mathcal{O}(e^2)$. The force $\boldsymbol{F}_{ij}$ and torque τ_{ij} exerted on particle i by particle j are given by

$$\boldsymbol{F}_{ij} = -\frac{\partial E_{ij}}{\partial L}\hat{\boldsymbol{e}}_{ij} = \frac{1}{3}e^4\pi\sigma\sin^8\theta\cos^2\theta\frac{c^6}{L^5}\cos\left[2(\alpha_i+\alpha_j-2\chi_{ij})\right]\hat{\boldsymbol{e}}_{ij}\,, \tag{11}$$

$$\tau_{ij} = -\frac{\partial E_{ij}}{\partial \alpha_i} = -\frac{1}{6}e^4\pi\sigma\sin^8\theta\cos^2\theta\frac{c^6}{L^4}\sin\left[2(\alpha_i+\alpha_j-2\chi_{ij})\right]\,, \tag{12}$$

with the unit vector $\hat{\boldsymbol{e}}_{ij}$ connecting the centers of particles i and j. As the Reynolds numbers are very small, we model the particle response to $\boldsymbol{F}_{ij}$, τ_{ij} as dominated by Stokes drag, so that particle i translates and rotates with velocity $\boldsymbol{v}_i$ and angular velocity Ω_i according to

$$\boldsymbol{v}_i = \sum_{j=1}^{M}\frac{1}{6\pi\beta\eta c}\boldsymbol{F}_{ij} \quad \text{and} \quad \Omega_i = \sum_{j=1}^{M}\frac{1}{8\pi\beta\eta c^3}\tau_{ij}\,. \tag{13}$$

The factor β is the fraction of the particle surface area subjected to drag. In the case of a gas-liquid interface, $\beta = (1+\cos\theta)/2$ to consistent leading order. In the simulations, the particle positions are advanced by $\Delta\boldsymbol{r}_i = \boldsymbol{v}_i\Delta t$ during a time step Δt, and the particle orientation by $\Delta\alpha_i = \Omega_i\Delta t$. From (13), the time scale t_{trans} needed for translation through a distance c is larger than the time scale t_{rot} needed to rotate through an angle of order 1, as $t_{trans} \sim (L/c)t_{rot}$. Particles therefore tend to adjust to locally optimal angles of orientation quasi-statically while translating, except when very close to other particles.

Dendritic structures. – The eventual pattern of particle aggregates depends on the details of particle interaction within the aggregates. If the particles are assumed "sticky" (freezing their position and orientation once they make contact), dendritic structures as shown in fig. 3 evolve. Dendrites were produced using both the explicit contact line integration and the analytical approach, with very similar results. In fig. 3 we show a calculation for $M = 1000$ particles with the analytical inter-particle potential. A wide variety of relative orientations $\Delta\alpha_{ij} = (\alpha_i - \alpha_j)$ of neighboring particles i and j (fig. 3c) is observed. This is to be expected, as these particles settle into locally optimal orientations with respect to their nearest neighbor. Because of the effects of next-nearest neighbors, a slight preference for director alignment ($\Delta\alpha_{ij} \approx 0$) can be seen.

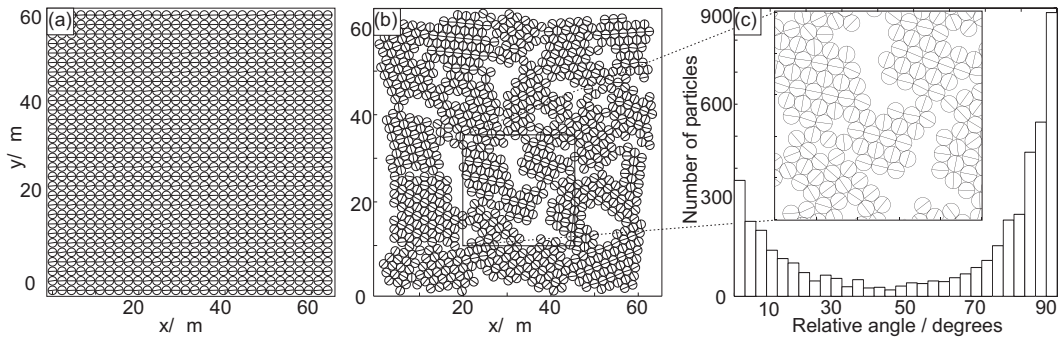

Fig. 4 – Raft structure: (a) initial configuration for simulation ($e = 0.10$); (b) end result of simulation (10000 seconds); (c) corresponding distribution of relative orientations with a zoom from (b) showing hexagonal packing with herringbone particle alignment.

Raft and lattice structures. – A different class of pattern emerges when the inter-particle potential is "non-sticky", *i.e.* all particles are free to rotate and translate at all times. This is achieved by adding a short-range repulsion, such as the generic short-range correction to quadrupolar capillary interactions discussed in [15]. Under these conditions, the particles tend to form "rafts". Particles interacting by quadrupolar forces may be expected to arrange in a square grid, as proposed in [15, 16]. Figure 4 shows the result of a quasi-static simulation starting with the centers of $M = 900$ particles in a square pattern, and a $\pm 5°$ variation in director angles. Contrary to expectation, the system evolves away from this initial configuration, developing instead a *hexagonal positional order*. This arrangement allows particles to fill space more efficiently (inter-particle distances are smaller).

With quadrupolar particles, hexagonal order does not allow for energetically optimal orientations. Instead, the *orientational order* that develops is of the *herringbone* type [17, 18], with directors of neighboring particles aligned in rows, but stacked at about 90° between two rows (fig. 4b). The relative orientations $\Delta\alpha_{ij}$ near 0° and 90° are strongly favored. In a perfect herringbone structure, each particle has two neighbours with $\Delta\alpha = 0°$ and four with $\Delta\alpha = 90°$; this $1:2$ ratio is also present in the distribution of fig. 4c.

The herringbone phase has been discussed recently in the context of molecular crystals and Langmuir monolayers [17, 18], and it has been shown that it is the low-temperature ground state for molecules with quadrupolar interaction [19]. Our simulations show that this phase develops on a much larger (micron) scale as well. As the simulations are conducted at $T = 0$, the resulting raft is not perfect, but consists of "crystallites" of herringbone order with unannealed voids between them (fig. 4b). When simulations are repeated with different short-range repulsion terms, the features of translational and orientational order persist. We conclude that short-range corrections to the quadrupolar potential are not crucial for the development of these patterns.

Conclusions. – The shape-induced potential described here is substantial ($> k_B T$) even for very small eccentricity ($e = 0.14$ corresponds to 10 nm deformations of 1 μm particles from spherical shape), so that it will nearly always be present in experiment. For typical material parameters (air/water interface, particle density $1050\,\mathrm{kg/m^3}$) and $e = 0.14$, $\theta = 120°$, shape-induced forces are dominant for radii in the range $0.3\,\mu\mathrm{m} < c < 10\,\mu\mathrm{m}$ (larger particles experience stronger forces by gravitational interface deformation, while thermal motion destroys aggregates for smaller sizes). For the conditions of the recent experiment by Loudet *et al.* [5], shape-induced forces are even expected to dominate gravitational forces up to $c \approx 35\,\mu\mathrm{m}$.

Loudet *et al.*'s observations that particles approaching tip-to-tip do so with $L(t) \propto t^{1/6}$ along a mostly straight trajectory are consistent with our results (note that (11) and (13) demand $\mathrm{d}L/\mathrm{d}t \propto L^{-5}$). However, it must be noted that the particles in that experiment greatly exceed the eccentricity for which our approximations and simulations are valid.

The relatively rapid $1/L^4$ decay of the potential (10) makes it an unlikely candidate to explain a much-discussed secondary potential minimum of long-range like-charged particle attraction beyond the reach of electrostatic repulsion [20]. It could, however, factor in the explanation of a secondary minimum at smaller distances [21]. We predict that the effect is largest for certain contact angles ($\theta \approx 63^\circ$ for partially wetting particles). Also, since the particle shape *imposes* the interfacial deformation, the shape interaction is stronger with *increasing* surface tension σ. These characteristics help in detecting the presence of shape interactions in experiment (the potential in [6], for instance, becomes weaker with increasing σ). While sticky particles form dendrites, non-sticky ones form rafts. Raft aggregates show hexagonal positional order and a peculiar herringbone orientational order. A quadrupolar interaction potential clearly allows hexagonal patterns and such ordering cannot, therefore, distinguish between isotropic and quadrupolar potentials.

REFERENCES

[1] PIERANSKI P., *Phys. Rev. Lett.*, **45** (1980) 569.
[2] MEJÍA-ROSALES S. J., GÁMEZ-CORRALES R., IVLEV B. I. and RUIZ-GARCÍA J., *Physica A*, **276** (2000) 30.
[3] RUIZ-GARCÍA J., GÁMEZ-CORRALES R. and IVLEV B. I., *Phys. Rev. E*, **58** (1998) 660.
[4] RUIZ-GARCÍA J., unpublished results.
[5] LOUDET J. C., ALSAYED A. M., ZHANG J. and YODH A. G., *Phys. Rev. Lett.*, **94** (2005) 018301.
[6] CHAN D. Y. C., HENRY J. D. and WHITE L. R., *J. Colloid Interface Sci.*, **79** (1981) 410.
[7] STAMOU D., DUSCHL C. and JOHANNSMANN D., *Phys. Rev. E*, **62** (2000) 5263.
[8] GOLESTANIAN R., GOULIAN M. and KARDAR M., *Phys. Rev. E*, **54** (1996) 6725.
[9] GOULIAN M., BRUINSMA R. and PINCUS P., *Europhys. Lett.*, **22** (1993) 145.
[10] WEISSTEIN E. W., `http://mathworld.wolfram.com/MeanCurvature.html` (2005).
[11] PRESS W. H. *et al.*, *Numerical Recipes: The Art of Scientific Computing* (Cambridge University Press, Cambridge, UK) 2000.
[12] NICOLSON M. M., *Proc. Cambridge Philos. Soc.*, **45** (1949) 288.
[13] OETTEL M., DOMÍNGUEZ A. and DIETRICH S., *Phys. Rev. E*, **71** (2005) 051401.
[14] KIM K. S., NEU J. and OSTER G., *Phys. Rev. E*, **61** (2000) 4281.
[15] KRALCHEVKSY P. A., DENKOV N. D. and DANOV K. D., *Langmuir*, **17** (2001) 7694.
[16] DANOV K. D., KRALCHEVSKY P. A., NAYDENOV B. N. and BRENN G., *J. Colloid Interface Sci.*, **287** (2005) 121.
[17] WÜRGER A., *J. Chem. Phys.*, **112** (2000) 3897.
[18] KAGANER V. M. and OSIPOV M. A., *J. Chem. Phys.*, **109** (1998) 2600.
[19] FOURNIER J. B. and GALATOLA P., *Phys. Rev. E*, **65** (2002) 031601.
[20] QUESADA-PÉREZ M., MONCHO-JORDÁ A., MARTÍNEZ-LÓPEZ F. and HIDALGO-ÁLVAREZ R., *J. Chem. Phys.*, **115** (2001) 10897.
[21] GÓMEZ-GUZMÁN O. and RUIZ-GARCIA J., *J. Colloid Interface Sci.*, **291** (2005) 1.